A Two-Dimensional Channel Simulation Model for Shadowing Processes

Xiaodong Cai, *Member, IEEE*, and Georgios B. Giannakis, *Fellow, IEEE*

***Abstract*—A Gaussian random process with a given power spectral density (PSD) function can be modeled as a sum of sinusoids (SOS), and has been widely used to simulate Rayleigh-fading communication channels. The conventional one-dimensional (1-D) channel model cannot capture the spatial correlation of shadowing processes. We here develop a two-dimensional (2-D) SOS-based channel model to simulate the shadowing process. Three methods to fit the PSD of the simulated process to the true channel's PSD are explored. Performance of the proposed channel simulator is analyzed in terms of the autocorrelation function of the simulated shadowing process. Simulations illustrate the potential of the proposed channel simulation model.**

***Index Terms*—Channel model, shadowing, spatial correlation, sum of sinusoids.**

I. Introduction

MOBILE radio communication channels have been studied for a long period of time based on measurement data and analysis of radio wave propagation. Typically, the radio channel is subject to two multiplicative forms of variations: fading and shadowing. Fading is due to multipath propagation. Signals from different paths add constructively or destructively, which results in rapid fluctuation of the signal amplitude within the order of a wavelength. Fading is often modeled as a complex Gaussian random process whose autocorrelation function (ACF) is determined by its Doppler spectrum in urban areas, where there is no line of sight between the transmitter and the receiver. Shadowing, on the other hand, occurs over a relative large area with different levels of clutter on the propagation path, which is also referred to as log-normal shadowing because the signal levels (measured in dB) follow a Gaussian (normal) distribution with local mean depending on the separation distance between the transmitter and the receiver.

A number of computer simulation models have been proposed to simulate fading channels. Basically, a stationary Gaussian process can be generated by passing a sequence of white Gaussian random deviates through a filter whose frequency response is the square root of the Gaussian process' power spectral density (PSD) [9, p. 403]. This method has been applied to simulate multipath fading channels in [3]. However, this filtering method usually entails considerable computational burden, especially when the bandwidth of the Doppler spectrum is narrow. An alternative method is based on the fact that a Gaussian random process can be expressed as a sum of infinite number of sinusoids with random phases, and properly selected frequencies [15], . In practice, a finite number of sinusoids can be used to approximate a Gaussian process, which reduces complexity. For this reason, the method of sum of sinusoids (SOS) to simulate fading channel has been extensively investigated [7], [8], [10]–[12], [14], [17]. In [7], a Monte Carlo method is proposed to randomly generate the sinusoids frequencies, and wide-sense stationary uncorrelated scattering (WSSUS) channels are simulated. In [17], an efficient scheme that has low computational complexity is advocated to simulate WSSUS channels with correlated paths. In [11], the method of SOS is studied in more detail, and several approaches to determining the sinusoidal frequencies are developed. The statistical properties of channel simulation models are presented in [12], and a fast implementation scheme based on a look-up table is advocated in [10]. The very popular Jakes' channel simulation model [8] calculates the frequencies of the sinusoids based on a physical channel model with uniformly distributed scatterrers around a circle. By assuming that the random phases of the signals with the same Doppler frequency, but from different scatterrers are the same, Jakes came up with an efficient channel simulator. However, the channel waveform generated by the Jakes' model is nonstationary because of the underlying random phase assumption [14].

In simulating a fading process, it is sufficient to generate a one-dimensional (1-D) random function of time because the fading waveform changes very fast even when the mobile moves a little distance. However, since shadowing effects occur over a relatively large area, it is desirable to generate a two-dimensional (2-D) random Gaussian process with proper spatial correlation. This is particularly useful when one wants to evaluate the performance of handover [13], [18], and macro-diversity algorithms [2]. For example, suppose a mobile is moving along a closed route rather than a straight line, and we want to study how the system handles the handover. In this case, a 1-D shadowing process cannot be used because it cannot capture the correlation of the channel along this closed route.

In this paper, we propose a 2-D simulation model for shadowing processes based on the SOS model. We first obtain the

Manuscript received December 27, 2001; revised April 7, 2003, June 27, 2003, August 21, 2003, and September 4, 2003. This work was supported by the NSF Wireless Initiative Grant 9979443, and prepared through collaborative participation in the Communications and Networks Consortium sponsored by the U.S. Army Research Laboratory under the Collaborative Technology Alliance Program, Cooperative Agreement DAAD19-01-2-0011. The U.S. Government is authorized to reproduce and distribute reprints for Government purposes notwithstanding any copyright notation thereon. The views and conclusions contained in this document are those of the authors and should not be interpreted as representing the official policies, either expressed or implied, of the Army Research Laboratory or the U.S. Government.

The authors are with the Department of Electrical and Computer Engineering, University of Minnesota, Minneapolis, MN 55455 USA (e-mail: caixd@ece.umn.edu; georgios@ece.umn.edu).

Digital Object Identifier 10.1109/TVT.2003.819627

spatial power spectrum from the autocorrelation of the shadowing process. Sampling the spatial power spectrum, we determine spatial frequencies which are then used as frequencies of the sinusoidal waveforms. Three frequency sampling methods, named uniform sampling method (USM), nonuniform sampling (NUSM), and Monte Carlo sampling method (MCM), are presented. The performance of the resulting channel simulator is analyzed in terms of the average squared error (ASE) of the corresponding autocorrelation function.

II. Channel Model and Simulation Methods

A statistical model has been developed for the land mobile radio channel by Suzuki [16]. In Suzuki's model, the amplitude of the channel, $h(t)$, is a product of a Rayleigh process $\beta(t)$, and a log-normal process $\alpha(t)$ [11], [16]

$$h(t) = \alpha(t)\beta(t). \tag{1}$$

The Rayleigh distributed process $\beta(t)$ accounts for fading, and is the envelope of a complex Gaussian random process. Here it is assumed that the fading channel is frequency-nonselective, which is valid when the bandwidth of the transmitted signal is much smaller than the channel's coherence bandwidth. The effect of shadowing is captured by the log-normal process $\alpha(t)$, which can also be expressed as

$$\alpha(t) = e^{\mu(t)+\sigma\, s(t)} \tag{2}$$

where $s(t)$ is a real Gaussian random process with zero mean and unit variance, the local mean $\mu(t)$ reflects the effect of the path loss, and σ is the standard deviation of the lognormal process whose typical value in urban areas is 8–10 dB [4], [6], [8, p. 121]. Notice that Suzuki's channel model is a random function of time. As aforementioned in Section I, the 1-D process $\alpha(t)$ cannot correctly capture the spacial correlation when a mobile user is moving along a curve rather than a straight line. This motivates the following 2-D lognormal process that depends on the user's location (x, y)

$$\alpha(x, y) = e^{\mu(x,y)+\sigma\, s(x,y)} \tag{3}$$

where both the local mean $\mu(x, y)$, and the Gaussian process $s(x, y)$ are now functions of mobile's location. Note that the mobile can always obtain a 1-D process for its channel from $\alpha(x, y)$, by finding its location at time t. For example, given a starting point (x_0, y_0), moving direction and velocity, one can relate $\alpha(t)$ to $\alpha(x, y)$ by using the equations $x = x_0 + v_x t$, and $y = y_0 + v_y t$, where $v_x(v_y)$ is the mobile's velocity along $x(y)$ direction. If the user changes moving direction and velocity, no explicit equation can relate the location (x, y) to time t. However, in system simulation using the channel model (3), we always know the mobile's location at a given time, and can obtain $\alpha(t)$ from $\alpha(x, y)$. If the 1-D channel model $\alpha(t)$ is used in simulation, every mobile needs to generate its own 1-D process. Even when two mobiles are in the same location, their channels generated from their individual 1-D channel models may be different. Furthermore, a 2-D channel model is capable of capturing the spatial correlation of the channel. Hence, a mobile can move along any route and obtain its channel from the 2-D process $\alpha(x, y)$. If the 1-D channel is utilized, a mobile may not be able to obtain its channel with correct correlation, when it is moving along a curve instead of a straight line. Since $\mu(x, y)$ can be easily calculated from the transmitter-receiver distance, and the path loss exponent, we need to generate the 2-D Gaussian random process $s(x, y)$ to obtain $\alpha(x, y)$. Our objective here is to present a simulation model, and develop simulation methods for the Gaussian process $s(x, y)$ with a prescribed spatial autocorrelation function.

The simulation model for a Gaussian random process $s(t)$ based on the SOS method is a 1-D function of the time variable t [11]

$$\hat{s}(t) = \sum_{n=1}^{N} c_n \cos(2\pi\, f_n t + \theta_n) \tag{4}$$

where θ_n is a random variable uniformly distributed in [0, 2π). The constants $\{c_n\}_{n=1}^{N}$ and the frequencies $\{f_n\}_{n=1}^{N}$ can be computed from the PSD of the fading process. For most applications, a moderately large value of N (e.g., $N = 30$) can render the probability density function (pdf) of $\hat{s}(t)$ sufficiently close to the Gaussian pdf [9, p. 214]. The average squared-error between the ACF of $\hat{s}(t)$ and the ACF of the actual fading channel is very small [11]. As a result, the computational complexity of the SOS method is very low. Furthermore, a fast method for implementing (4) based on a look-up table is possible [10].

In order to account for the spatial correlation of the shadowing process, we extend the 1-D SOS-based channel model to the following 2-D channel simulation model for the Gaussian process $s(x, y)$

$$\hat{s}(x, y) = \sum_{n=1}^{N} c_n \cos\left[2\pi(f_{x,n}x + f_{y,n}y) + \theta_n\right]. \tag{5}$$

As in the 1-D simulation model of (4), $\{\theta_n\}_{n=1}^{N}$ are random variables uniformly distributed over [0, 2π). Here, we use two spatial frequencies f_x and f_y to sample the 2-D PSD of the Gaussian random process, which makes the simulation model have a 2-D ACF. Discrete spatial frequencies $\{f_{x,n}\}_{n=1}^{N}$ and $\{f_{y,n}\}_{n=1}^{N}$ can be either deterministic or randomly generated according to a specific pdf, while constants $\{c_n\}_{n=1}^{N}$ can be obtained from the spatial PSD of the shadowing process.

The number of sinusoids N in the 2-D simulation model of (5) is expected to be much larger than that in the 1-D model of a Rayleigh-fading channel, since we need to approximate a 2-D PSD using these sinusoids. Also, the pdf of $\hat{s}(x, y)$ should approach the Gaussian pdf of $s(x, y)$ with sufficient accuracy over a large region, which also requires a relatively large N. For the Rayleigh-fading channel $\beta(t)$, deep fading occurs around the zero value of $\beta(t)$. Thus, the pdf in a relatively narrow region around zero is important, when it comes to simulating the bit error rate (BER) performance of a communication system. For the shadowing process $\alpha(x, y)$ (or equivalently $\alpha(t)$) however, $\alpha(x, y)$ goes to zero, when $s(x, y)$ tends to negative infinity.

Hence, the pdf of $s(x,y)$ in the region where $s(x,y)<0$ is important. This may cause difficulties on accurate simulation of the shadowing process, since the pdf of $\hat{s}(x,y)$ may not exhibit sufficient accuracy at its left tail. However, the critical region that high accuracy is required for the pdf of $\hat{s}(x,y)$ is $\hat{s}(x,y)>d$, where d is an application-dependent constant. Since $P(s(x,y)<-5)=2.87\times10^{-7}$ ($P(\cdot)$ denotes the probability of the event in the paratheses.), it follows that $d=-5$ is sufficient for most applications. In other words, because the event $s(x,y)<-5$ has low probability, the simulated channel's pdf does not require high accuracy in the region $s(x,y)<-5$. For applications involving simulations of handover algorithms, we only need the outage probability of SNR, rather than the average BER. In such cases, d may take a larger value e.g., $d=-3$ (since $P(s(x,y)<-3)=1.3\times10^{-3}$), while still maintaining sufficient accuracy. The simulations in Section IV show that the cumulative distribution function (CDF) of our simulated channel $\hat{s}(x,y)$ is quite accurate over a wide region with a moderately large N. Furthermore, we can always increase N to achieve a desirable accuracy, since the pdf of $\hat{s}(x,y)$ approaches the Gaussian pdf, as N goes to infinity.

If the only random variables in (5) are $\{\theta_n\}_{n-1}^{N}$, the ACF of $\hat{s}(x,y)$ can be evaluated as

$$\begin{aligned}R_{\hat{s}}(\Delta x,\Delta y)&=E\left\{\hat{s}(x,y)\hat{s}(x+\Delta x,y+\Delta y)\right\}\\&=\sum_{n=1}^{N}\frac{c_n^2}{2}\cos\left[2\pi(f_{x,n}\Delta x+f_{y,n}\Delta y)\right].\end{aligned}\quad(6)$$

The corresponding PSD of $\hat{s}(x,y)$ is given by

$$\begin{aligned}\Phi_{\hat{s}}(f_x,f_y)=\sum_{n=1}^{N}\frac{c_n^2}{4}&\left[\delta(f_x-f_{x,n})\delta(f_y-f_{y,n})\right.\\&\left.+\delta(f_x+f_{x,n})\delta(f_y+f_{y,n})\right],\end{aligned}\quad(7)$$

where $\delta(\cdot)$ is the Dirac delta function. Because $\hat{s}(x,y)$ in (5) is Gaussian for every x and y when N is sufficiently large, the only problem here is in selecting c_n, $f_{x,n}$ and $f_{y,n}$ so that the error between $R_{\hat{s}}$ and R_s, the ACF of the actual shadowing process $s(x,y)$, is as small as possible. We shall develop three methods to calculate c_n, $f_{x,n}$ and $f_{y,n}$, namely USM, NUSM, MCM. In the MCM method, $f_{x,n}$ and $f_{y,n}$ are also random variables, so the ACF in (6), and the PSD in (7) are random functions conditioned on $f_{x,n}$ and $f_{y,n}$. To develop these methods, we need to know the ACF, and the PSD of the Gaussian process $s(x,y)$.

The ACF of the Rayleigh-fading channel is well studied by analyzing radio wave propagation. It is typically expressed by the zeroth order Bessel function of the first kind for land mobile radio channels. The ACF of the shadowing process is less well specified in the literature. However, an exponential ACF which fits well the measurement data is given by [6]

$$R_s(\Delta x,\Delta y)=R_s(d)=e^{-ad}\quad(8)$$

where a is a constant depending on the environment, and $d:=\sqrt{\Delta x^2+\Delta y^2}$ is the distance between two locations. Calculated from the data reported in [6], $a\approx0.1204$ for urban areas and $a\approx0.002$ for suburban areas. Performing 2-D Fourier transform on $R_s(\Delta x,\Delta y)$, we obtain the PSD (see Appendix for detailed derivations)

$$\Phi_s(f_x,f_y)=\frac{2\pi\,a}{\left[a^2+4\pi^2\left(f_x^2+f_y^2\right)\right]^{\frac{3}{2}}}.\quad(9)$$

We see that $\Phi_s(f_x,f_y)$ is circularly symmetric, and if we define f_r such that $f_x=f_r\cos(\theta)$ and $f_y=f_r\sin(\theta)$, then (9) becomes the 1-D transform of $R_s(d)$

$$\Phi_s(f_r)=\frac{2\pi\,a}{\left[a^2+4\pi^2f_r^2\right]^{\frac{3}{2}}}.\quad(10)$$

It is seen from (10) that $\Phi_s(f_r)$ has a low-pass characteristic. If we define its z-dB cutoff frequency f_c as $\Phi_s(f_c)/\Phi_s(0)=10^{-z/10}$, then $f_c=a(10^{2z/30}-1)/2\pi$. Based on (9) or (10), we can proceed to calculate the sample frequencies $f_{x,n}$ and $f_{y,n}$, and the constant c_n in the channel simulation model (5).

A. Uniform Sampling Method

In this method, we sample $\Phi_s(f_x,f_y)$ uniformly up to its cutoff frequency, similar to the method of equal distances used when simulating 1-D Rayleigh-fading channels [11]. Letting $\Delta f:=f_c/M$, we have the following frequency samples

$$\begin{aligned}\tilde{f}_{x,i}&=\frac{\Delta f}{2}(2i-1),\quad i\in[1,M],\\\tilde{f}_{y,j}&=\frac{\Delta f}{2}(2j-1),\quad j\in[-M+1,M].\end{aligned}\quad(11)$$

Note that due to the circular symmetry of $\Phi_s(f_x,f_y)$ in (9) and the structure of $\Phi_{\hat{s}}(f_x,f_y)$ in (7), we only need samples for $f_x>0$. The total number of frequency sampling points is $N=2M^2$. Defining $\nu:=n$ modulo $2M$, we obtain N sampling points as $\{(f_{x,n},f_{y,n}):f_{x,n}=\tilde{f}_{x,k},f_{y,n}=\tilde{f}_{y,l},k=\nu+1,l=n-(2\nu+1)M+1\}$. Now, let us consider the frequency region

$$\begin{aligned}I_n=\Bigg\{&(f_x,f_y):f_{x,n}-\frac{\Delta f}{2}\le f_x<f_{x,n}+\frac{\Delta f}{2},\\&f_{y,n}-\frac{\Delta f}{2}\le f_y<f_{y,n}+\frac{\Delta f}{2}\Bigg\}.\end{aligned}\quad(12)$$

The mean power of $s(x,y)$ in this region is given by (13), which can be evaluated using (14) [1, eq. 3.3.49], where A, B, c, d are constants. Because the mean power of $\hat{s}(x,y)$ in the region I_n should be equal to that of $s(x,y)$, from (7) and (13), we have $A_n^2=c_n^2/4$; thus, $c_n=2A_n$. Finally, to normalize the variance of $\hat{s}(x,y)$, we use $c_n=A_n/\sqrt{\sum_{n=1}^{N}A_n^2}$. Since we sample $\Phi_s(f_x,f_y)$ uniformly, $R_{\hat{s}}(\Delta x,\Delta y)$ is a periodic function of Δx and Δy with period $1/\Delta f$, or equivalently, M/f_c. Note that the simulated random process $\hat{s}(x,y)$ in (5) is itself a periodic function of x and y. Hence, the simulated channel $\hat{s}(x,y)$ obtained with USM is valid within a distance of half period: $M/(2f_c)$.

To enlarge the operational range of our model, we develop a nonuniformly sampling method in the next subsection.

$$A_n^2 = \int\int_{I_n} \Phi_s(f_x, f_y) df_x df_y = \int_{f_{y,n}-\frac{\Delta f}{2}}^{f_{y,n}+\frac{\Delta f}{2}} \frac{2\pi a}{a^2 + 4\pi^2 f_y^2} \times \left(\frac{f_{x,n} + \frac{\Delta f}{2}}{\sqrt{a^2 + 4\pi^2 \left[\left(f_{x,n} + \frac{\Delta f}{2} \right)^2 + f_y^2 \right]}} - \frac{f_{x,n} - \frac{\Delta f}{2}}{\sqrt{a^2 + 4\pi^2 \left[\left(f_{x,n} - \frac{\Delta f}{2} \right)^2 + f_y^2 \right]}} \right) df_y \quad (13)$$

$$\int \frac{dx}{(Ax^2 + B)(cx^2 + d)^{\frac{1}{2}}} = \frac{1}{[B(Ad - Bc)]^{\frac{1}{2}}} \times \arctan \frac{x(Ad - Bc)^{\frac{1}{2}}}{[B(cx^2 + d)]^{\frac{1}{2}}} \quad \text{for } Ad > Bc \quad (14)$$

B. Nonuniform Sampling Method

The mean power within the cutoff frequency is given by $P = \int_0^{2\pi} \int_0^{f_c} \Phi_s(f_r) f_r df_r d\theta = 2\pi \int_0^{f_c} \Phi_s(f_r) f_r df_r$. In the nonuniform sampling method, we first find M frequencies $\{f_{r,m}\}_{m=1}^M$ such that

$$\int_0^{2\pi} \int_{f_{r,m-1}}^{f_{r,m}} \Phi_s(f_r) f_r df_r d\theta = \frac{P}{M} \quad (15)$$

where we let $f_{r,0} = 0$. Then, we pick up $2M$ angles uniformly distributed in $(-(\pi/2), (\pi/2)) : \varphi_i = \pi(2i - 2M + 1)/4M$, $i = 0, 1, \ldots, 2M - 1$. The sampling frequencies are $f_{x,n} = f_{r,k} \cos(\varphi_l)$ and $f_{y,n} = f_{r,k} \sin(\varphi_l)$, where $k = \nu + 1$, and $l = n - 2\nu M$. Here, we sample $\Phi_s(f_x, f_y)$ uniformly along half circles because of the circular symmetry of the PSD; the sampling along the frequency f_r is nonuniform, but the power in between $f_{r,m-1}$ and $f_{r,m}, m = 0, 1, \ldots M$ is equal. By doing so, the coefficient $c_n = \sqrt{2/N}$ has the same value for each sampling point. Hence, NUSM is similar to the method of equal areas used in simulating a 1-D Gaussian random process [11]. It can be shown that

$$\int_0^{2\pi} \int_{f_{r,m-1}}^{f_{r,m}} \Phi_s(f_r) f_r df_r d\theta = \frac{a}{\sqrt{a^2 + 4\pi^2 f_{r,m-1}^2}} - \frac{a}{\sqrt{a^2 + 4\pi^2 f_{r,m}^2}}. \quad (16)$$

Combining (15) and (16), we can compute recursively the frequency $f_{r,m}$ as follows:

$$f_{r,m} = \frac{1}{2\pi} \sqrt{\left(\frac{P}{Ma} + \frac{1}{a^2 + 4\pi^2 f_{r,m-1}^2} \right)^{-2} - a^2}. \quad (17)$$

The period of $\hat{s}(x, y)$ is the least common multiple of the period of $\cos[2\pi(f_{x,n}x + f_{y,n}y)]$. Because of the nonuniform sampling of $f_{x,n}$ and $f_{y,n}$, the period of $\hat{s}(x, y)$ is much larger than that of the uniform sampling method. This is very useful when we need to simulate the shadowing effect in a large suburban area.

C. Monte Carlo Method

The sampling frequencies $(f_{x,n}, f_{y,n})$ in USM and NUSM are deterministic variables, and only the phases are randomly generated. In the MCM method, the discrete frequencies $(f_{x,n}, f_{y,n})$ are generated according to a given joint pdf, $p_{F_x,F_y}(f_x, f_y)$, which is related to the PSD of the shadowing process. For the 1-D simulation model in (4), it has been shown that the sampling frequencies f_n can be generated according to a pdf proportional to the PSD of $s(t)$ [7]. Following the procedure in [7], we can also show that the joint pdf $p_{F_x,F_y}(f_x, f_y)$ in our 2-D simulation model is proportional to the 2-D PSD (see Appendix for detailed derivations)

$$p_{F_x,F_y}(f_x, f_y) = b\, \Phi_s(f_x, f_y), \quad f_x > 0 \quad (18)$$

where the constant $b := 1/\int_{-\infty}^{\infty} \int_0^{\infty} \Phi_s(f_x, f_y) df_x df_y$ normalizes the pdf. For the normalized $\Phi_s(f_x, f_y)$, we have $\int_{-\infty}^{\infty} \int_{-\infty}^{\infty} \Phi_s(f_x, f_y) df_x df_y = 1$, and thus $b = 2$. Directly generating $(f_{x,n}, f_{y,n})$ according to the joint pdf in (18) is difficult. However, if we change variables (F_x, F_y) to (F_r, Θ) by $F_x = F_r \cos(\Theta)$ and $F_y = F_r \sin(\Theta)$, the joint pdf of F_r and Θ is given by

$$p_{F_r,\Theta}(f_r, \theta) = \frac{2\pi ab f_r}{[a^2 + 4\pi^2 f_r^2]^{\frac{3}{2}}}. \quad (19)$$

From (19), we see that F_r and Θ are two independent random variables: Θ is uniformly distributed in $[-\pi/2, \pi/2)$, while F_r is distributed according to (19) multiplied by π. So we can independently generate the random variables F_r and Θ according to their pdfs, and then obtain (F_x, F_y) using the circular to Cartesian transformation that relates them. The CDF of the random variable F_r is found as

$$P_{F_r}(f_r) = 1 - \frac{a}{\sqrt{a^2 + 4\pi^2 f_r^2}}. \quad (20)$$

From (20), the random variable F_r can be generated based on a random variable u which is uniformly distributed over [0, 1) as follows:

$$f_r = P_{F_r}^{-1}(u) = \frac{a}{2\pi} \sqrt{\frac{1}{(1-u)^2} - 1}. \quad (21)$$

The coefficients $\{c_n\}_{n=1}^N$ have the same value: $c_n = \sqrt{2/N}$, $\forall n$.

Because the discrete frequencies $(f_{x,n}, f_{y,n})$ are randomly generated, the period of the simulated process $\hat{s}(x, y)$ by MCM is expected to be much larger than that of $\hat{s}(x, y)$ generated by

using the USM. Since both frequencies and phases are randomly generated, MCM yields a process that has additional degrees of freedom and statistical characteristics close to the true Gaussian process, which we will justify in the next section.

D. Implementation Issues

Implementation of our 2-D channel simulator involves much more computation than the 1-D fading channel simulator, because many more sinusoids are needed to sample the 2-D PSD of the shadowing process. The 1-D fast-fading channel simulator is often used to simulate the link level performance of a wireless system in real time, or, in computer simulations. Therefore, it is necessary to have an efficient means of implementing the channel simulator, and the Jakes' simulator offers a very good alternative. However, the shadowing effect of the channel usually affects performance of the system level algorithms such as handover. Because the system level simulation is much more complicated, it is usually carried out by computer simulation. The 2-D channel simulator we developed is intended for such simulations, in which case its complexity is not a major concern. Therefore, we will not pursue sophisticated schemes to reduce the computational burden at a level comparable to the Jakes' model. But it is worth pointing out that it is straightforward to reduce e.g., the computation of USM by exploiting the uniformity of its sampling frequencies. For the USM, using (11), we can express the simulated random process in (5) as

$$\hat{s}(x,y)=\sum_{n=1}^{M}\sum_{m=1}^{M}c_{n,m}\left\{\cos\left[2\pi(\tilde{f}_{x,n}x+\tilde{f}_{y,m}y)+\theta_{n,m}\right]+\cos\left[\tilde{f}_{x,n}x-\tilde{f}_{y,m}y)+\tilde{\theta}_{n,m}\right]\right\} \quad (22)$$

which can also be written as

$$\hat{s}(x,y)=\sum_{n=1}^{M}\sum_{m=1}^{M}c_{n,m}\cos\left[2\pi\, f_{x,n}x+\frac{(\theta_{n,m}+\tilde{\theta}_{n,m})}{2}\right]\times\cos\left[2\pi\, f_{y,m}y+\frac{(\theta_{n,m}-\tilde{\theta}_{n,m})}{2}\right]. \quad (23)$$

Defining $\psi_{m,n}:=(\theta_{m,n}+\tilde{\theta}_{m,n})/2$, and $\tilde{\psi}_{m,n}:=(\theta_{m,n}-\tilde{\theta}_{m,n})/2$, we can rewrite (23) as (24), which is shown at the bottom of the page. Based on (24), the channel simulator can be implemented by using only $4M$ sinusoidal waveforms instead of $2M^2$ sinusoids, which substantially reduces computation. We can also simplify the implementation of the channel simulator that uses NUSM based on the symmetry property of some sampling frequencies. As for MCM, since the sampling frequencies are random variables, it turns out that we should use N sinusoidal waveforms to generate the channel. As a result, MCM has the highest computational complexity.

$$\hat{s}(x,y)=\sum_{n=1}^{M}\sum_{m=1}^{M}c_{n,m}\left[\cos(2\pi\, f_{x,n}x)\cos\psi_{n,m}-\sin(2\pi\, f_{x,n}x)\sin\psi_{n,m}\right]\times\left[\cos(2\pi\, f_{y,m}y)\cos\tilde{\psi}_{n,m}-\sin(2\pi\, f_{y,m}y)\sin\tilde{\psi}_{n,m}\right]. \quad (24)$$

III. Performance Evaluation

Both CDF and ACF of the simulated channel are important performance measures. We will show the CDF of the simulated channel in Section IV. In this section, we will focus on the ACF of the simulated channel. After a brief discussion on the ergodicity of ACF, we will analyze the average squared error between the ACFs of $\hat{s}(x,y)$ and $s(x,y)$.

$$\tilde{R}_{\hat{s}}(\Delta x,\Delta y)=\lim_{\substack{X\to\infty\\ Y\to\infty}}\frac{1}{2X}\frac{1}{2Y}\times\int_{-X}^{X}\int_{-Y}^{Y}\hat{s}(x,y)\hat{s}(x+\Delta x,y+\Delta y)dydx \quad (25)$$

In the 2-D channel simulation model (5), once the random numbers θ_n (and ($f_{x,n}$, $f_{y,n}$) for MCM) are generated, we obtain a realization of the simulated random process. It is clear that the time average of each realization is zero, which implies that the simulated random process is mean-ergodic. A more important property is the ergodicity of the autocorrelation function. If the simulation model is autocorrelation-ergodic, theoretically speaking, it is not necessary to generate different realizations to simulate the second-order statistics of the channel, when a user moves through a very large area. Let us define the spatially averaged estimate of the ACF as (25), shown at the bottom of the page, where X and Y determine the size of the area over which $\tilde{R}_{\hat{s}}(\Delta x,\Delta y)$ is estimated. It is straightforward to show that

$$\tilde{R}_{\hat{s}}(\Delta x,\Delta y)=R_{\hat{s}}(\Delta x,\Delta y). \quad (26)$$

Notice that $\tilde{R}_{\hat{s}}(\Delta x,\Delta y)$ and $R_{\hat{s}}(\Delta x,\Delta y)$ [cf. (6)] are deterministic for USM and NUSM, while they are random for MCM because they are functions of the frequencies ($f_{x,n}$, $f_{y,n}$). From (26), we see that the simulated random processes generated by using USM and NUSM are autocorrelation-ergodic. From this point of view, once the random phases have been generated, we do not need to generate them again, when the user moves through a large area. However, it is worth emphasizing here that we need to generate many channel realizations to capture the distribution function of the channel, since a channel realization is a deterministic function of time once the random phases (and random frequencies in MCM) are generated. Thus, ergodicity of the ACF does not reduce simulation complexity without sacrificing CDF performance.

In MCM, because the frequencies ($f_{x,n}$, $f_{y,n}$) are also random variables, $R_{\hat{s}}(\Delta x,\Delta y)$ defined in (6) is a random function conditioned on ($f_{x,n}$, $f_{y,n}$). To obtain the true ACF, $R_{\hat{s},m}(\Delta x,\Delta y)$, we need to take expectation on the conditional ACF $R_{\hat{s}}(\Delta x,\Delta y)$ with respect to the random frequencies ($f_{x,n}$, $f_{y,n}$), that is

$$R_{\hat{s},m}(\Delta x,\Delta y)=\int_{-\infty}^{\infty}\int_{0}^{\infty}R_{\hat{s}}(\Delta x,\Delta y)p_{F_x,F_y}(f_x,f_y)df_xdf_y. \quad (27)$$

Because the pdf $p_{F_x,F_y}(f_x,f_y)$ is chosen according to (18), we have $R_{\hat{s},m}(\Delta x,\Delta y)=R_s(\Delta x,\Delta y)$. On the other hand, the ACF of the simulated channel using USM or NUSM is given by (6), which is not equal to $R_s(\Delta x,\Delta y)$. Hence, as far the

second-order statistics are concerned, MCM is the best method to simulate the fading process $s(x,y)$, although for each realization its time average autocorrelation $\tilde{R}_{\hat{s}}(\Delta x,\Delta y)$ may have larger error compared with USM or NUSM, as we will observe in the simulation results of the next section. Because the time average autocorrelation function is not equal to the true ACF, i.e., $\tilde{R}_{\hat{s}}(\Delta x,\Delta y)\neq R_{\hat{s},m}(\Delta x,\Delta y)$, the shadowing process generated by using MCM is not autocorrelation-ergodic. Therefore, it is required to generate many realizations by randomly selecting the phases θ_n, and the frequencies $(f_{x,n},\ f_{y,n})$. Note that this does not increase the simulation burden, since many channel realizations are required to capture the channel CDF.

The channel simulation model in (5) uses a finite number of sinusoids, which implies that we can only sample the PSD at a limited number of points. This results in the difference between the ACF of the simulated channel, and the ACF of the true channel. As a figure of merit, we will consider the following average squared error (ASE) between the ACF of simulated process $\hat{s}(x,y)$, and the ACF of the true fading process $s(x,y)$

$$ASE=\frac{1}{4XY}\times\int_{-X}^{X}\int_{-Y}^{Y}\left[R_{\hat{s}}(\Delta x,\Delta y)-R_s(\Delta x,\Delta y)\right]^2 d\Delta x d\Delta y. \quad (28)$$

Note that ASE is a deterministic number for USM and NUSM, while it is a random variable for MCM. The ASE can be evaluated using numerical integration. However, when X and Y are large, it is not feasible to perform 2-D numerical integration. In the following, we will develop upper and lower bounds for ASE, which will turn out to be very tight when X and Y are sufficiently large. we will let $X=Y$ because the autocorrelation function is circularly symmetric. The ASE in (27) can be written

$$ASE=T_1-2T_2+T_3 \quad (29)$$

where we define

$$T_1=\frac{1}{4X^2}\int_{-X}^{X}\int_{-X}^{X}R_{\hat{s}}^2(\Delta x,\Delta y)d\Delta x d\Delta y \quad (30)$$

$$T_2=\frac{1}{4X^2}\int_{-X}^{X}\int_{-X}^{X}R_{\hat{s}}(\Delta x,\Delta y)R_s(\Delta x,\Delta y)d\Delta x d\Delta y \quad (31)$$

and

$$T_3=\frac{1}{4X^2}\int_{-X}^{X}\int_{X}^{X}R_s^2(\Delta x,\Delta y)d\Delta x d\Delta y. \quad (32)$$

Let us partition the set $I:=\{(f_{x,n},f_{y,n})\times(f_{x,m},f_{y,m}):\forall n\neq m\}$ into five disjoint subsets: $I_1:=\{(f_{x,n},f_{y,n})\times(f_{x,m},f_{y,m}):f_{x,n}\neq f_{x,m},f_{y,n}\neq f_{y,m},f_{y,n}\neq -f_{y,m},\forall n\neq m\}$; $I_2:=\{(f_{x,n},f_{y,n})\times(f_{x,m},f_{y,m}):f_{x,n}=f_{x,m},f_{y,n}\neq f_{y,m},f_{y,n}\neq -f_{y,m},\forall n\neq m\}$; $I_3:=\{(f_{x,n},f_{y,n})\times(f_{x,m},f_{y,m}):f_{x,n}=f_{x,m},f_{y,n}=-f_{y,m},\forall n\neq m\}$; $I_4:=\{(f_{x,n},f_{y,n})\times(f_{x,m},f_{y,m}):f_{x,n}\neq f_{x,m},f_{y,n}=f_{y,m},\forall n\neq m\}$; and $I_5:=\{(f_{x,n},f_{y,n})\times(f_{x,m},f_{y,m}):f_{x,n}\neq f_{x,m},f_{y,n}=-f_{y,m},\forall n\neq m\}$. After cumbersome but straightforward manipulations on (29), we obtain

$$\begin{aligned}T_1=&\frac{1}{8}\sum_{n=1}^{N}c_n^4+\frac{1}{4X^2}\sum_{n=1}^{N}\frac{c_n^4}{8}\frac{1}{4\pi^2 f_{x,n}f_{y,n}}\\&\times\sin(4\pi f_{x,n}X)\sin(4\pi f_{y,n}X)\\&+\frac{1}{2X}\sum_{I_2,I_3}\frac{c_n^2c_m^2}{8}\frac{\sin\left(2\pi(f_{y,n}-f_{y,m})X\right)}{\pi(f_{y,n}-f_{y,m})}\\&+\frac{1}{4X^2}\sum_{I_1,I_2,I_4}\frac{c_n^2c_m^2}{8}\\&\times\frac{\sin\left(2\pi(f_{x,n}+f_{x,m})X\right)\sin\left(2\pi(f_{y,n}+f_{y,m})X\right)}{\pi^2(f_{x,n}+f_{x,m})(f_{y,n}+f_{y,m})}\\&+\frac{1}{2X}\sum_{I_3,I_5}\frac{c_n^2c_m^2}{8}\frac{\sin\left(2\pi(f_{x,n}+f_{x,m})X\right)}{\pi(f_{x,n}+f_{x,m})}\\&+\frac{1}{4X^3}\sum_{I_1,I_5}\frac{c_n^2c_m^2}{8}\\&\times\frac{\sin\left(2\pi(f_{x,n}-f_{x,m})X\right)\sin\left(2\pi(f_{y,n}-f_{y,m})X\right)}{\pi^2(f_{x,n}-f_{x,m})(f_{y,n}-f_{y,m})}\\&+\frac{1}{2X}\sum_{I_4}\frac{c_n^2c_m^2}{8}\frac{\sin\left(2\pi(f_{x,n}-f_{x,m})X\right)}{\pi(f_{x,n}-f_{x,m})}. \quad (33)\end{aligned}$$

Let $B_1:=(4X^2)\int_{-\infty}^{\infty}\int_{-\infty}^{\infty}R_s(\Delta x,\Delta y)R_{\hat{s}}(\Delta x,\Delta y)d\Delta x d\Delta y$ and $B_2:=(4X^2)^{-1}\sum_{n=1}^{N}2c_n^2\int_X^{\infty}\int_X^{\infty}R_s(\Delta x,\Delta y)d\Delta x d\Delta y$. Since $|\cos(\alpha)|\leq 1$, we have $B_1-B_2<T_2<B_1+B_2$. Substituting (6) and (8) into the definition of B_1, we obtain

$$B_1=\frac{1}{4X^2}\sum_{n=1}^{N}\frac{a\pi c_n^2}{\left[a^2+4\pi^2\left(f_{x,n}^2+f_{y,n}^2\right)\right]^{\frac{3}{2}}}. \quad (34)$$

Because $R_s(\Delta x,\Delta y)>0$, we have

$$\begin{aligned}B_2&<\frac{1}{4X^2}\sum_{n=1}^{N}2c_n^2\int_0^{2\pi}\int_X^{\infty}R_s\left(r\cos(\theta),r\sin(\theta)\right)r dr d\theta\\&=\frac{1}{4X^2}\frac{4\pi}{a}e^{-aX}\left(X+\frac{1}{a}\right)\sum_{n=1}^{N}c_n^2=:B_3 \quad (35)\end{aligned}$$

We thus obtain an upper and a lower bound for T_2, which are: $T_{2U}=B_1+B_3$ and $T_{2L}=B_1-B_3$, respectively. The bounds of T_3 can be obtained as follows:

$$\begin{aligned}T_3&>\frac{1}{4X^2}\int_0^{2\pi}\int_0^{X}R_s^2\left(r\cos(\theta),\ r\sin(\theta)\right)r\,dr d\theta\\&=\frac{1}{4X^2}\left[\frac{\pi}{2a^2}-e^{-2aX}\frac{\pi}{a}\left(X+\frac{1}{2a}\right)\right]=:T_{3L} \quad (36)\end{aligned}$$

and

$$\begin{aligned}T_3&<\frac{1}{4X^2}\int_0^{2\pi}\int_0^{\sqrt{2}X}R_s^2\left(r\cos(\theta),\ r\sin(\theta)\right)r\,dr d\theta\\&=\frac{1}{4X^2}\left[\frac{\pi}{2a^2}-e^{-2\sqrt{2}aX}\frac{\pi}{a}\left(\sqrt{2}X+\frac{1}{2a}\right)\right]=:T_{3U} \quad (37)\end{aligned}$$

Finally, the upper bound and the lower bound for the ASE are given by $ASE_U=T_1-2T_{2L}+T_{3U}$ and $ASE_L=T_1-2T_{2U}+$

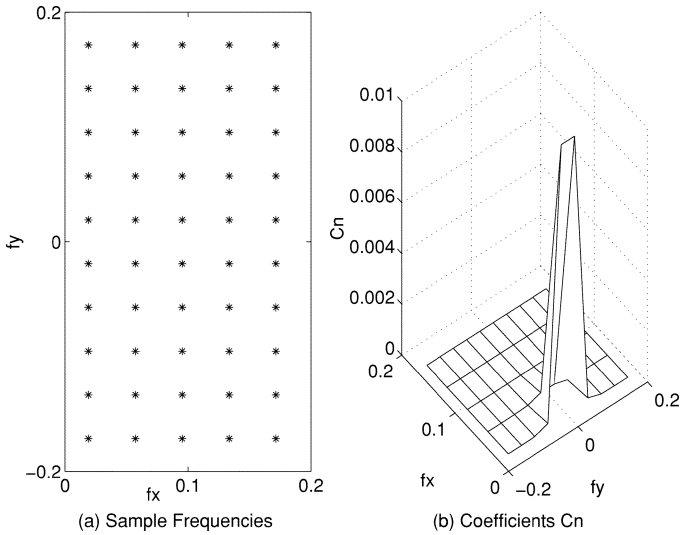

Fig. 1. Sample frequencies and coefficients of USM.

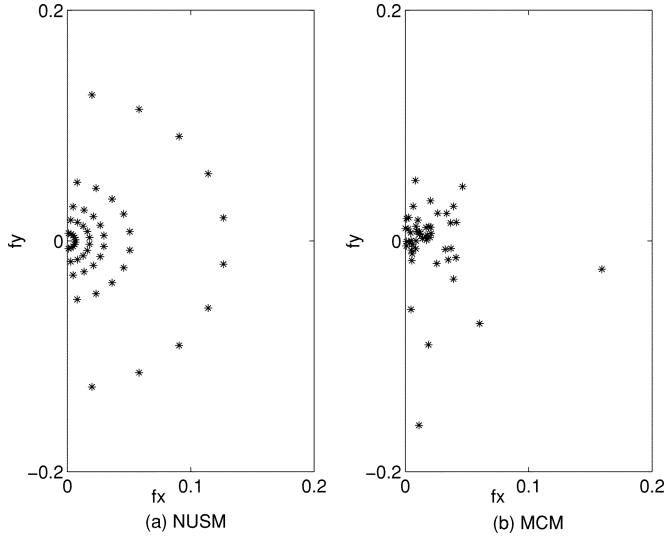

Fig. 2. Sample frequencies of NUSM and MCM.

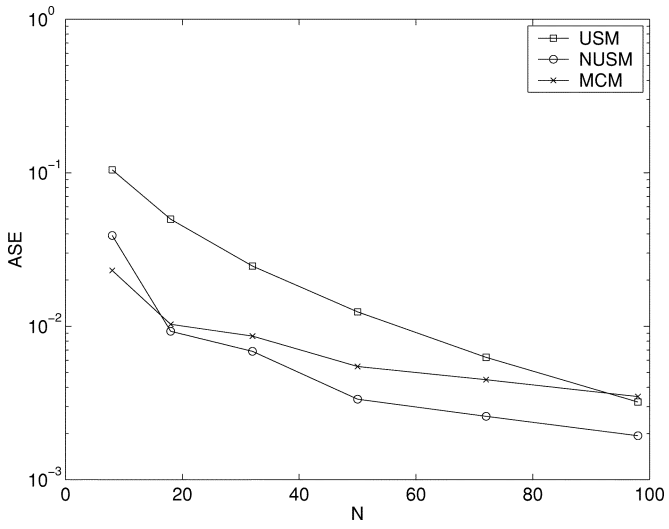

Fig. 3. Average squared error of ACF versus number of frequency samples.

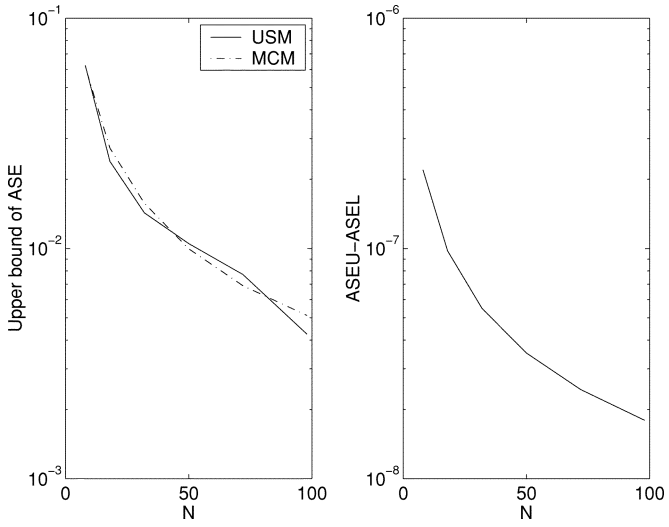

Fig. 4. Bounds of average squared error of ACF.

T_{3L}. The difference between the upper bound and lower bound is

$$ASE_U - ASE_L = 4B_3 + T_{3U} - T_{3L}. \tag{38}$$

When X is sufficiently large, i.e., $aX \gg 1$, the difference is very small. In this case, we can evaluate the ASE of the ACF by using either the upper or the lower bound.

IV. Numerical Results

In this section, we present numerical results for the channel simulation models with model parameters obtained by USM, NUSM, and MCM. We simulate the shadowing process in the urban scenario, where the correlation is reported to be 0.3 when the distance is 10 m [6]. We use a 30-dB cutoff frequency; i.e., the amplitude of the PSD in (10) at the cutoff frequency is 30 dB lower than the amplitude at frequency zero. The 30-dB cutoff frequency in this particular case can be found as $f_c = 0.19\,\mathrm{period/m}$. The number of sampling frequencies is chosen as $N = 50$ in all plots.

Fig. 1 shows the sampling frequencies and the coefficients of the sinusoids for USM, while Fig. 2 depicts the sampling frequencies for NUSM and MCM. As we mentioned before, the sampling frequencies of NUSM are nonuniformly distributed along the radius, but are uniformly distributed along semicircles in the 2-D frequency plane. The sampling frequencies of MCM are random numbers; here, we show a realization of these random frequencies. Fig. 3 demonstrates the ASE between the theoretical ACF $R_s(\Delta x, \Delta y)$ and the ACF of the simulated process $R_{\hat{s}}(\Delta x, \Delta y)$, which is obtained from (28) by using numerical integration. The average is taken with $X = Y = M/(2f_c)$ with $M = 5$. In MCM, the ASE is obtained by averaging over 100 realizations with randomly generated sampling frequencies. We observe from Fig. 3 that NUSM has the smallest ASE. However, it is unfair to compare the ASE of USM and NUSM with the ASE of MCM. Because the ACF of MCM is the same as the theoretical ACF, the ASE of MCM can be interpreted as the average variance. On the other hand, the ASE of USM and NUSM is the averaged bias. The upper bounds of ASE of NUSM and MCM are shown in Fig. 4, where the spa-

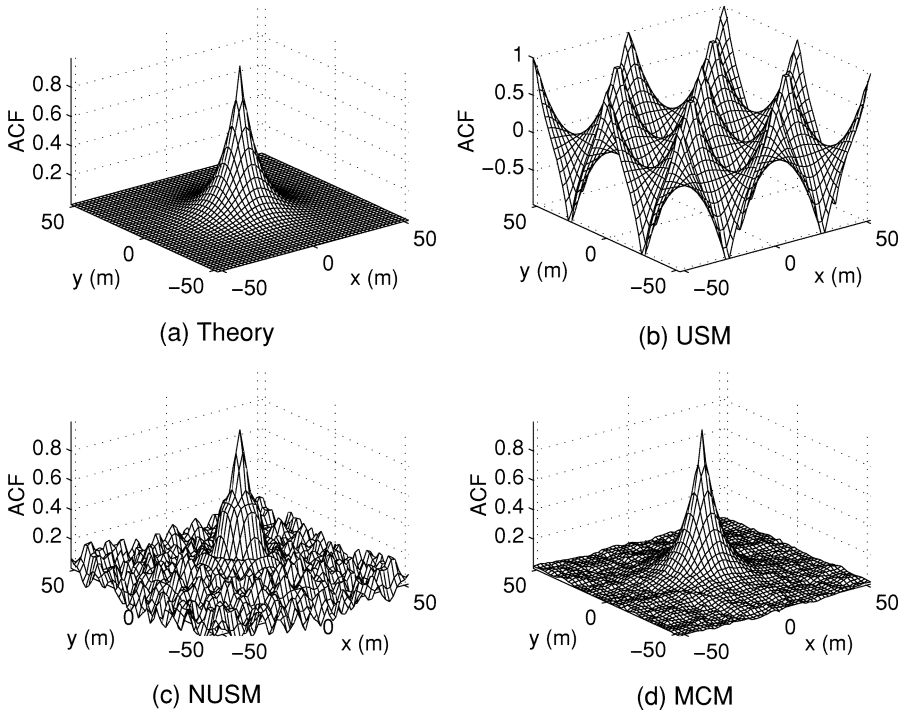

Fig. 5. 2-D ACFs of theoretical and simulated processes.

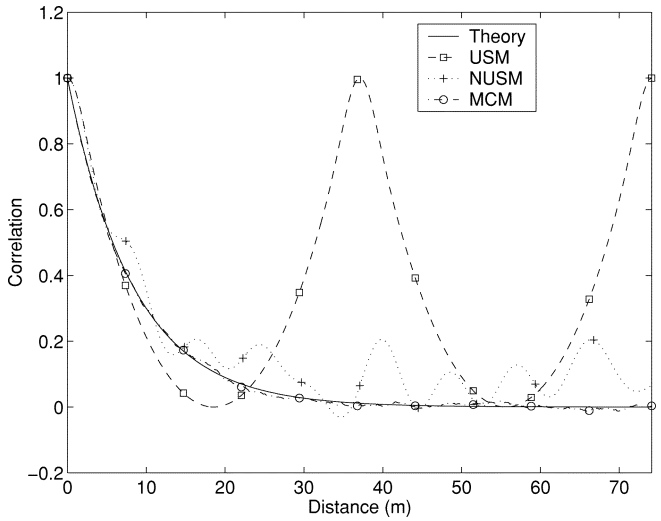

Fig. 6. 1-D ACFs of theoretical and simulated processes.

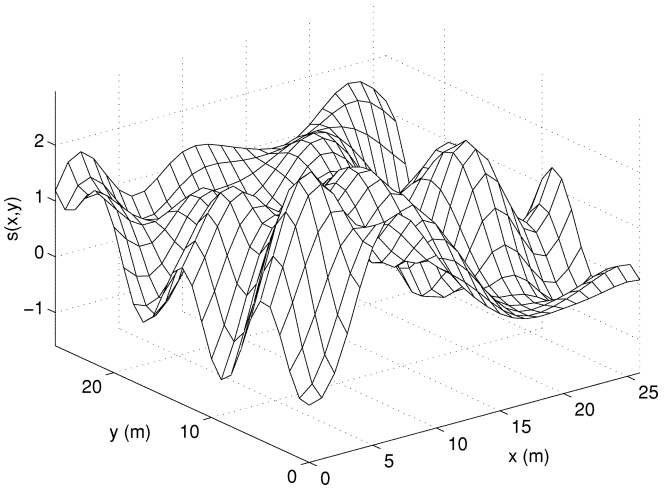

Fig. 7. A realization of the 2-D simulated Gaussian process using USM.

tial average is over $X = Y = 20/f_c$ to ensure $aX \gg 1$, and the upper bound in MCM is averaged over 100 runs. The difference between the upper and the lower bound is also shown in Fig. 4. It is seen that the difference is very small, and thus the bound is very close to the true ASE. We note that the ASE shown in Fig. 3 is slightly different from the upper bound shown in Fig. 4 although the upper bound is very tight. This is because the areas we take to compute the ASE are different in the two cases. The 2-D ACFs, as well as the 1-D ACFs along the line $\Delta x = \Delta y$, are shown in Figs. 5 and 6. The ACF of MCM is an approximate ACF obtained by averaging over 100 realizations. It is clear from Figs. 5 and 6 that the ACF in USM is a periodic function. The averaged ACF in MCM is very close to the theoretical ACF, confirming our argument in the last section that the ACF in MCM is the same as the theoretical ACF.

A 2-D realization of the simulated process using NUSM is shown in Fig. 7, and a 1-D realization along a circle of radius 10 m is shown in Fig. 8. From Fig. 8, we see that the simulated process has the same value in the beginning and at the end, since the process at these two points is from the same location. If we use the 1-D channel simulation model $\hat{s}(t)$ given by (4), the ACF of $\hat{s}(t)$ is a function of Δt. If the mobile is moving along a straight line, the ACF of $\hat{s}(t)$ reflects correctly the spatial correlation. However, if the mobile is moving along a curve, $\hat{s}(t)$ is unable to capture the spatial correlation of the channel. When the mobile moves along a closed curve and comes back to the starting point after a certain period of time, the channel generated from the 1-D model at the starting time and at the end time may be completely uncorrelated even if the mobile is in the same location. Finally, Fig. 9 depicts the CDFs of the simulated channels, which are obtained from 10^6 realizations of

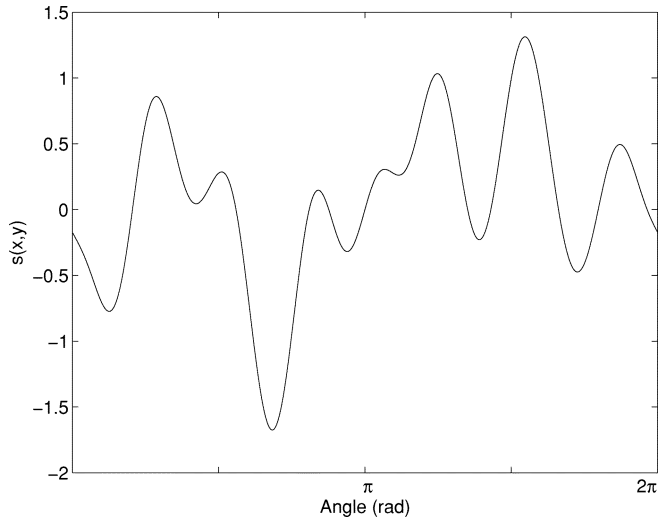

Fig. 8. A realization of the 1-D simulated Gaussian around a circle.

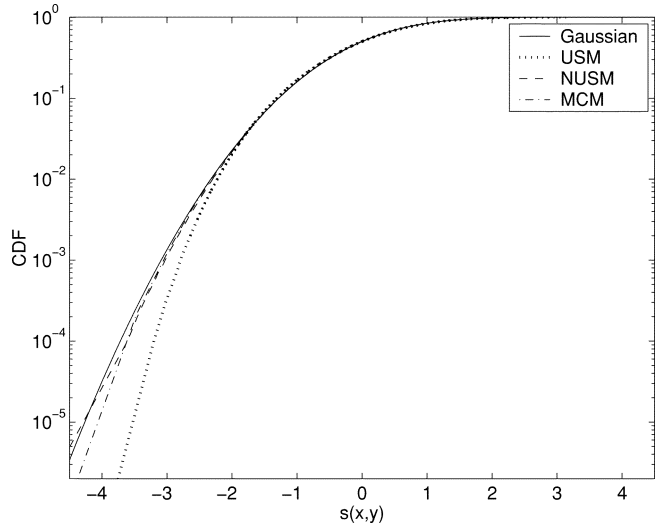

Fig. 9. Comparison between CDFs of the simulated processes and the Gaussian CDF.

each simulated channel. We see that when NUSM or MCM is used, the CDF is quite accurate. However, if USM is used in the simulation, the CDF is accurate in a limited region. This is due to the following reason: the coefficients $\{c_n\}_{n=1}^{N}$ have the same value in NUSM or MCM, while they are unequal in USM. Since only several coefficients have relatively large value in USM, the effective number of sinusoids decreases, which degrades the accuracy of the CDF of the simulated channel. Hence, NUSM and MCM outperform USM in terms of the distribution function of the simulated channel.

V. Conclusion

In this paper, we derived a 2-D channel simulation model for the shadowing process based on the sum of sinusoids method. The proposed model is capable of capturing the 2-D spatial correlation of the channel. Three schemes were developed to implement the simulation, among which the USM is the simplest but has a limited operational range for the simulated process, while the MCM exhibits the best performance in terms of the autocorrelation function, but has the highest complexity. A compromise between performance and complexity is offered by NUSM. The proposed 2-D simulation model for the shadowing process has high application potential for studying algorithms involving handover and marco-diversity in wireless systems.

Appendix

I. Derivation of (9)

Taking 2-D Fourier transform of the autocorrelation function, we have

$$\begin{aligned}\Phi_s(f_x,f_y) &= \int_{-\infty}^{\infty}\int_{-\infty}^{\infty} e^{-a\sqrt{x^2+y^2}} e^{-j(2\pi f_x x+2\pi f_y y)}dxdy \\ &= \int_0^{2\pi}\int_0^{\infty} e^{-[a+j2\pi(f_x\cos\theta+f_y\sin\theta)]r}\, r\, drd\theta \\ &= \int_0^{2\pi} \frac{1}{[a+j2\pi(f_x\cos\theta+f_y\sin\theta)]^2}d\theta. \end{aligned} \tag{39}$$

Letting $f_x = f_r\cos(\varphi)$ and $f_x = f_r\sin(\varphi)$, (39) becomes

$$\Phi_s(f_x,f_y) = \int_0^{2\pi} \frac{1}{[a+j2\pi\, f_r\cos(\theta-\varphi)]^2}d\theta. \tag{40}$$

Since the integrand is a periodic function, we obtain

$$\begin{aligned}\Phi_s(f_x,f_y) &= \int_0^{2\pi} \frac{1}{[a+j2\pi\, f_r\cos(\theta)]^2}d\theta \\ &= \int_0^{2\pi} \frac{a^2-4\pi^2 f_r^2\cos^2\theta + j4\pi\, a f_r\cos\theta}{\left(a^2+4\pi^2 f_r^2\cos^2\theta\right)^2}d\theta \\ &= \int_0^{2\pi} \frac{a^2-4\pi^2 f_r^2\cos^2\theta}{\left(a^2+4\pi^2 f_r^2\cos^2\theta\right)^2}d\theta \end{aligned} \tag{41}$$

where the imaginary part of the integral is zero, because $\cos(\theta)$ is antisymmetric around $\theta=\pi$. Using the identity $\cos^2(\theta) = [1+\cos(2\theta)]/2$, and letting $x = 2\theta$, we can write (41) as

$$\Phi_s(f_x,f_y) = \int_0^{2\pi} \frac{a^2-2\pi^2 f_r^2 - 2\pi^2 f_r^2\cos(x)}{\left(a^2+2\pi^2 f_r^2+2\pi^2 f_r^2\cos(x)\right)^2}dx. \tag{42}$$

Using the formulas

$$\int_0^{2\pi} \frac{A+B\cos x}{(c+d\cos x)^2}\,dx = \frac{Ac-Bd}{c^2-d^2}\int_0^{2\pi}\frac{1}{c+d\cos x}dx \tag{43}$$

and [5, p. 168]

$$\int \frac{1}{c+d\cos x}dx = \frac{2}{\sqrt{c^2-d^2}}\arctan\frac{\sqrt{c^2-d^2}\tan\left(\frac{x}{2}\right)}{c+d} \tag{44}$$

for $c^2 > d^2$, we obtain

$$\Phi_s(f_r) = \frac{2\pi a}{[a^2+4\pi^2 f_r^2]^{\frac{3}{2}}}. \tag{45}$$

□

II. Derivation of (18)

The ACF of the simulated channel using the MCM can be obtained from (6) as shown in (46), where we use the fact that $\{f_{x,n}, f_{y,n}\}_{n=1}^{N}$ are independent and identically distributed. Since the ACF is the inverse Fourier transform of the PSD, we have (47), where we used the circular symmetry property of the PSD $\Phi_s(f_x, f_y)$. Since we need to guarantee that $R_{\hat{s},m}(\Delta x, \Delta y) = R_s(\Delta x, \Delta y)$, comparing (46) with (47), we must have $p_{F_x,F_y}(f_x, f_y) = 2\Phi_s(f_x, f_y)/\sum_{n=1}^{N} c_n^2/4$. Since $\sum_{n=1}^{N} c_n^2/2 = \int_{-\infty}^{\infty}\int_{-\infty}^{\infty} \Phi_s(f_x, f_y) df_x, df_y$, and $\Phi_s(f_x, f_y)$ is symmetric with respect the x-axis, we arrive at (18). □

$$\begin{aligned} R_{\hat{s},m}(\Delta x,\ \Delta y) &:= E\left\{R_{\hat{s}}(\Delta x,\ \Delta y)\right\} \\ &= \sum_{n=1}^{N} \frac{c_n^2}{2} E\frac{\{\cos\left[2\pi(f_{x,n}\Delta x + f_{y,n}\Delta y)\right]\}}{N} \\ &= \sum_{n=1}^{N} \frac{c_n^2}{4} \int_{-\infty}^{\infty}\int_{0}^{\infty} p_{F_x,F_y}(f_x, f_y) \\ &\quad \times \left[e^{j2\pi(f_x\Delta x + f_y\Delta y)} + e^{-j2\pi(f_x\Delta x + f_y\Delta y)}\right] \\ &\quad \times df_x df_y \end{aligned} \tag{46}$$

$$\begin{aligned} R_s(\Delta x,\ \Delta y) &= \int_{-\infty}^{\infty}\int_{-\infty}^{\infty} \Phi_s(f_x,\ f_y) e^{j2\pi(f_x\Delta x + f_y\Delta y)} df_x\, df_y \\ &= \int_{-\infty}^{\infty}\int_{0}^{\infty} \Phi_s(f_x,\ f_y) \\ &\quad \times \left[e^{j2\pi(f_x\Delta x + f_y\Delta y)} + e^{-j2\pi(f_x\Delta x + f_y\Delta y)}\right] \\ &\quad \times df_x\, df_y \end{aligned} \tag{47}$$

References

[1] M. Abramowitz and I. A. Stegun, *Handbook of Mathematical Functions with Formulas, Graphs, and Mathematical Tables*. Washington, DC: National Bureau of Standards, 1972.

[2] R. C. Bernhardt, "Macroscopic diversity in frequency reuse radio systems," *IEEE J. Select. Areas Commun.*, vol. 11, pp. 1013–1023, Sept. 1993.

[3] S. A. Fechtel, "A novel approach to modeling and efficient simulation of frequency-selective fading radio channels," *IEEE J. Select. Areas Commun.*, vol. 11, pp. 422–431, Apr. 1993.

[4] A. J. Goldsmith, L. J. Greenstein, and G. J. Foschini, "Error statistics of real-time power measurements in cellular channels with multipath and shadowing," *IEEE Trans. Veh. Technol.*, vol. 43, pp. 439–446, Aug. 1994.

[5] I. S. Gradshtein and I. Ryzhik, *Table of Integrals, Series, and Products*. San Diego, CA: Academic, 2000.

[6] M. Gudmundson, "Correlation model for shadowing fading in mobile radio systems," *Electron. Lett.*, vol. 27, pp. 2145–2146, Nov. 1991.

[7] P. Höeher, "A statistical discrete-time model for the WSSUS multipath channel," *IEEE Trans. Vel. Technol.*, vol. 41, pp. 461–468, Nov. 1992.

[8] W. C. Jakes, *Microwave Mobile Communications*. New York: Wiley, 1974.

[9] A. Papoulis, *Probability, Random Variables, and Stochastic Processes*. New York: McGraw-Hill, 1991.

[10] M. Patzöld, R. Farcía, and F. Laue, "Design of high-speed simulation models for mobile fading channels by using table look-up techniques," *IEEE Trans. Veh. Technol.*, vol. 49, pp. 1178–1190, July 2000.

[11] M. Patzöld, U. Killat, and F. Laue, "A deterministic digital simulation model for Suzuki processes with application to a shadowed Rayleigh land mobile radio channel," *IEEE Trans. Veh. Technol.*, vol. 45, pp. 318–331, May 1996.

[12] M. Patzöld, U. Killat, F. Laue, and Y. Li, "On the statistical properties of deterministic simulation models for mobile fading channels," *IEEE Trans. Veh. Technol.*, vol. 47, pp. 254–269, Feb. 1998.

[13] G. Pollini, "Trends in handover design," *IEEE Comm. Mag.*, vol. 34, pp. 82–90, Mar. 1996.

[14] M. F. Pop and N. C. Beaulieu, "Limitation of sum-of sinusoids fading channel simulators," *IEEE Trans. Commun.*, vol. 49, pp. 699–708, Apr. 2001.

[15] S. O. Rice, "Mathematical analysis of random noise," *Bell Syst. Tech. J.*, vol. 23, pp. 282–332, July 1944.

[16] S. O. Rice, "Mathematical analysis of random noise," *Bell Syst. Tech. J.*, vol. 23, pp. 46–156, Jan. 1945.

[17] K.-W. Yip and T.-S. Ng, "Efficient simulation of digital transmission over WSSUS channels," *IEEE Trans. Commun.*, vol. 43, pp. 2907–2913, Dec. 1995.

[18] N. Zhang and J. M. Holtzman, "Analysis of handoff algorithms using both absolute and relative measurements," *IEEE Trans. Veh. Technol.*, vol. 45, pp. 174–179, Feb. 1996.

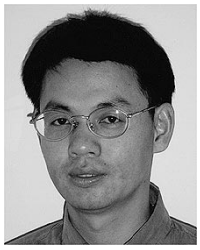

Xiaodong Cai (M'01) received the B.S. degree from Zhejiang University, China, the M.Eng. degree from the National University of Singapore, Singapore, and the Ph.D. degree from the New Jersey Institute of Technology, Newark, in 2001, all in electrical engineering.

From February 2001 to June 2001, he was a Member of Technical Staff at Lucent Technologies, NJ, working on WCDMA project; from July 2001 to October 2001, he was a Senior System Engineer with the Sony Technology Center, San Diego, CA, where he was involved in developing high data rate wireless modem. Since November 2001, he has been a Postdoctoral Research Associate with the Department Of Electrical And Computer Engineering, University of Minnesota. His research interests include communication theory, signal processing, and wireless networks.

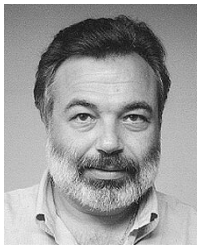

Georgios B. Giannakis (F'97) received the Diploma in electrical engineering from the National Technical University of Athens, Greece, in 1981. He received the M.Sc. degree in electrical engineering in 1983, the M.Sc. degree in mathematics in 1986, and the Ph.D. degree in electrical engineering, also in 1986, from the University of Southern California (USC).

After lecturing for one year at USC, he joined the University of Virginia in 1987, where he became a Professor of Electrical Engineering in 1997. Since 1999, he has been a Professor with the Department of Electrical and Computer Engineering at the University of Minnesota, where he now holds an ADC Chair in Wireless Telecommunications. His general interests span the areas of communications and signal processing, estimation and detection theory, time-series analysis, and system identification—subjects on which he has published more than 175 journal papers, 325 conference papers, and two edited books. Current research focuses on transmitter and receiver diversity techniques for single- and multiuser fading communication channels, complex-field and space–time coding, multicarrier, ultrawide-band wireless communication systems, cross-layer designs, and distributed sensor networks.

Dr. Giannakis is the (co-)recipient of four Best Paper Awards from the IEEE Signal Processing (SP) Society (1992, 1998, 2000, 2001). He also received the Society's Technical Achievement Award in 2000. He served as Editor-in-Chief of the IEEE Signal Processing Letters, as Associate Editor for the IEEE Transactions on Signal Processing, and the IEEE Signal Processing Letters, as secretary of the SP Conference Board, as member of the SP Publications Board, as member and vice-chair of the Statistical Signal and Array Processing Technical Committee, as chair of the SP for Communications Technical Committee, and as a member of the IEEE Fellows Election Committee. He is currently a member of the IEEE-SP Society's Board of Governors, the Editorial Board for the Proceedings of the IEEE, and chairs the steering committee of the IEEE Transactions on Wireless Communications.